Journal of Alloys and Compounds 509 (2011) 3141–3147

Contents lists available at ScienceDirect

Journal of Alloys and Compounds

journal homepage: www.elsevier.com/locate/jallcom

Structure and mechanical properties of (TiVCr)N coatings prepared by energetic bombardment sputtering with different nitrogen flow ratios

Du-Cheng Tsai, Yen-Lin Huang, Sheng-Ru Lin, De-Ru Jung, Shou-Yi Chang, Fuh-Sheng Shieu*

Department of Materials Science and Engineering, National Chung Hsing University, Taichung 402, Taiwan

ARTICLE INFO

Article history:
Received 17 August 2010
Received in revised form 2 December 2010
Accepted 3 December 2010
Available online 10 December 2010

Keywords:
Coating materials
Nitride materials
Thin films
Vapor deposition
Crystal structure

ABSTRACT

The (TiVCr)N coatings were deposited on Si substrate via rf magnetron sputtering of a TiVCr alloy target under dc bias in a N_2/Ar atmosphere. The deposition rate of the coatings gradually decreased with increasing N_2-to-total (N_2 + Ar) flow ratio, R_N. The TiVCr alloy and its nitride coatings exhibited a body-centered cubic (BCC) and a face-centered cubic (FCC) crystal structure, respectively. The preferred orientation of the (TiVCr)N coatings changed from (1 1 1) to (2 0 0) with increasing R_N. In addition, the microstructure of the nitride coatings was also converted from a columnar structure with void boundaries and rough-faceted surface to a very dense structure with a smooth-domed surface. The grain size of the (TiVCr)N coatings decreased as the R_N was increased. Accordingly, the hardness of the (TiVCr)N coatings was enhanced from 4.06 to 18.74 GPa as the R_N was increased.

1. Introduction

In the past decade, binary transition metal nitrides and carbides have been widely used as hard protective coatings. These have also been applied to tools for cutting and forming, to machinery components, aerospace and automotive parts, among others due to their high hardness, wear resistance, thermal stability, oxidation resistance, and chemical stability [1–4]. To enhance the performance of particular tools, dies, and molds for several applications, hard coating technology is continually being developed.

Multi-elemental coatings with different metallic and nonmetallic alloying elements have been developed in recent years. The combined attributes of individual components provide better mechanical performance. The best known example of this is the incorporation of Al atoms with a TiN and CrN lattice, which has been successfully commercialized particularly for high speed machining applications because of its significantly improved oxidation resistance and hardness over TiN and CrN. Chen et al. have reported that the addition of Al significantly increases hardness from 24 GPa with TiN to 31.2 GPa with the TiAlN coating. After vacuum thermal annealing at 900 °C, the hardness of TiAlN coatings remains quite constant [5]. Chim et al. measured the hardness of TiAlN and CrAlN coatings at different temperatures. They found that the high hardness (37 GPa) of the as-deposited TiAlN coating can be retained for annealing temperature up to 600 °C, and the high hardness (35 GPa) of the CrAlN coating is maintained up for an annealing temperature of 800 °C [6]. Keunecke et al. and Ding et al. also reported the formation of super hard TiAlN (41.6 GPa) and CrAlN (40 GPa) films, respectively [7,8]. These results clearly show that TiN or CrN coatings alloyed with Al have significantly enhanced hardness and thermal stability [9–12]. Moreover, great effort has also been done by alloying nitride coatings with other elements, such as Ti–Cr–N, Ti–Zr–N, Ti–Ta–N, and Cr–Zr–N. TiCrN coating has previously shown the superior oxidation resistance [13]. Vishnyakov et al. showed that the hardness value of deposited TiCrN coating can achieve 31 GPa [14]. The TiZrN coatings have excellent hardness ranging from 35.5 to 37.5 GPa [15]. Moreover, an earlier study on the effects of Zr implantation on TiN coatings has shown improved wear resistance [16]. For the Ti–Ta–N system, a maximum hardness of 42 GPa is observed [17]. Kim et al. confirmed the superior mechanical property of the CrZrN coatings (32.5 GPa) compared with CrN (22 GPa) [18]. The two common extrinsic hardening mechanisms in ternary nitrides are solid solution hardening and grain boundary hardening. In the first mechanism, the incorporated solid solution atoms serve as centers of distortion and the resulting stress field reacts with the elastic stress field of a dislocation, leading to solid solution hardening. In the second hardening mechanism, the mutual incorporation of differently sized atoms leads to a decrease in grain size, indicating a high density of grain boundaries. An increase in the density of the grain boundaries diminishes dislocation activity, resulting in grain boundary hardening.

* Corresponding author at: Department of Materials Science and Engineering, National Chung Hsing University, Taichung 40227, Taiwan. Tel.: +886 4 2284 0500; fax: +886 4 2285 7017.
E-mail address: fsshieu@dragon.nchu.edu.tw (F.-S. Shieu).

0925-8388/$ – see front matter © 2010 Elsevier B.V. All rights reserved.
doi:10.1016/j.jallcom.2010.12.026

An alloy system called "high-entropy alloys", with the addition of multi-principal elements, has been recently developed; this system possesses simple solid solutions with nanocrystalline and even amorphous structures [19,20]. Four core effects, namely, high entropy, sluggish diffusion, severe lattice distortion, and cocktail effects, have also been proposed to constitute the multi-principal elemental effect of high-entropy alloys on microstructure, phase transformation, and their properties. In brief, high entropy plays an important role in simplifying microstructures so that they principally consist of simple solid solution phases with face-centered cubic (FCC) and body-centered cubic (BCC) structures. Lattice distortion influences mechanical, physical, and chemical properties. Sluggish diffusion leads to alloys developing nanocrystalline or even amorphous structures. Finally, the cocktail effects result in a composite effect on properties wherein the interactions among the different elements themselves play an important role. For example, $Al_xCoCrCuFeNi$ alloys with different Al contents possess simple solid solution structures. Except for the FCC (Cu-rich) interdendrite, the crystal structure is transformed from FCC to BCC with an increase in aluminum content. These alloys exhibit promising mechanical properties, including excellent elevated-temperature strength and good wear resistance [21,22]. $Al_xCoCrFeNi$ alloys with different Al contents have also been fabricated by Li et al. They confirm that Al promotes the formation of BCC structure especially when Cu is absent. The increase in Al content leads to distortion of the crystalline lattice and alloy strengthening [23]. AlCoCrCuFeNi alloys demonstrate excellent room-temperature compressive strengths [24]. Moreover, the microstructure and mechanical properties of the various alloying techniques with different alloying elements have been investigated in detail [25,26]. Deposition from high-entropy alloy targets has been considered based on these bulk properties to produce multi-component alloys, nitrides, and carbides. Recent studies involving TiVCrZrY, AlCrTaTiZr, AlCrNbSiTiV, and TiAlCrNbY display simple solid solution structures and outstanding mechanical properties. These alloy coatings exhibit a hardness ranging from 6.8 to 13 GPa, which is higher than that of conventional metallic elements and binary alloys [27–30]. The hardness of the TiVCrZrY nitride coating reaches 17.5 GPa when deposited without substrate bias and/or heating [27], whereas AlCrTaTiZr and AlCrNbSiTiV nitride coatings possess high hardness values up to 35 and 41 GPa under biased and heated conditions, respectively [28,29]. A TiAlCrNbY carbide coating using separate, pure metallic Ti, Al, Cr, Nb, and Y targets is reportedly softer (23.5 GPa) than aforementioned nitrides, but has superior tribological performance [30]. These confirm that the multi-component coatings are effective in increasing hardness.

Based on the aforementioned mechanisms, these mechanical properties can be expected of quaternary nitride (TiVCr)N, such that the three elements, Ti, V, and Cr, are employed to manufacture the target alloy in this study. In previous papers, TiVCr alloy coatings produced simple BCC solid solutions from all alloyed elements and achieved a hardness of 11 GPa [31]. This confirms that a coating of the present alloy design effectively increases hardness. During sputtering deposition, a dc bias is applied to the substrates to obtain a denser structure. The structure of the coatings can be controlled accordingly by varying the N_2 flow ratio (R_N). Consequently, the effect of R_N on the structures and physical properties of deposited (TiVCr)N coatings, including crystal structures and microstructures, as well as the mechanical property, was examined.

2. Experimental

The (TiVCr)N coatings were deposited on p-Si (1 0 0) wafers via an rf magnetron sputtering system using equimolar TiVCr targets 50 mm in diameter. Before deposition, the Si substrates were cleaned, and then rinsed with ethanol and distilled water in an ultrasonic bath. The deposition of the (TiVCr)N coatings was carried out at room temperature in an $Ar + N_2$ atmosphere under an rf power of 150 W and a working pressure of 6×10^{-3} Torr. During deposition, the total gas flow ratio was fixed to 30 sccm and the N_2-to-total flow ratio (R_N, i.e., the ratio between the flow rates of N_2 and total (N_2 + Ar) mixture) was varied from 0% to 50%. Deposition time was increased with increasing R_N so as to control the coating thickness at around 500 nm. The targets were presputtered via Ar to remove their surface oxide layers before deposition. Details of the process parameters are listed in Table 1.

Table 1
Deposition conditions of the (TiVCr)N coatings.

Process parameter	Values
Base pressure (Torr)	8×10^{-6}
Working pressure (Torr)	6×10^{-3}
rf power (W)	150
Ar flow (sccm)	30, 27, 24, 21, 18, 15
N_2 flow (sccm)	0, 3, 6, 9, 12, 15
R_N (%)	0, 10, 20, 30, 40, 50
Bias (V)	−100
Deposition temperature	Room temperature

The chemical compositions of the (TiVCr)N coatings were determined by field-emission electron probe microanalyses (FE-EPMA, JOEL JXA-8800M). At least three tests were performed for each sample. The crystal structures were analyzed by glancing-incidence (1°) X-ray diffractometer (XRD, BRUKER D8 Discover) using Cu Kα radiation at a scanning speed of 1°/min. The scanning step was 0.01° and the scanning range was 20–80°. Furthermore, from the full width at half-maximum, the average grain sizes of the coatings were calculated with Scherrer's formula [32]. The morphology studies and thickness measurements were carried out using field emission scanning electron microscopy (SEM, JEOL JSM-6700F). Meanwhile, the deposition rate can be obtained by dividing the thickness with deposition time. Microstructural examinations were conducted using an analytical transmission electron microscope (TEM, JEM 1200EX II). The specimen for TEM examination was mechanically polished and then cut into a suitable size, approximately 5 mm × 5 mm for mounting. Planar or cross-sectional specimens were initially thinned mechanically to ~100 μm, followed by attachment to a copper grid using a G1 epoxy bond (Gatan G1, Gatan Inc., USA). Thinning to electron transparency was then performed using a Gatan model 691 precision ion polishing system (PIPS). The PIPS system was equipped with two ionic milling guns that generate inert (Ar) ionic or atomic beams under high voltage (4 kV beams at 4°) to thin the specimens from both sides until perforation. The surface morphology of the coatings was observed under an atomic force microscope (AFM, Seiko SPA400). The surface roughness (root-mean-square) values of the coatings were derived from the AFM images. The microhardness and elastic modulus of the coatings were measured using a TriboLab nanoindenter (Hysitron). During the tests, an applied load of 50–2000 μN was set. A maximum load of 900 μN was then selected based on the test results to maintain the penetration depth below 1/10 of film thickness, thereby neglecting the substrate effect. At least five tests were performed for each sample.

3. Results and discussion

3.1. Crystal structures and crystallinity

Fig. 1 plots the FE-EPMA elemental content of the (TiVCr)N alloy deposited at various R_N. The composition of the deposited coatings deviated from the designed values of the TiVCr target with equimolar elements. The difference in the composition of each element between target and coatings can be related to the sequence of the sputtering yield Cr > V > Ti [33]. Generally, one component of an alloy or mixture can be expected to sputter faster than the other components, leading to an enrichment of that component in the deposited film and resulting in a deposited film with a different composition than that of the target. A similar phenomenon is reported in NiTi thin films deposited from an equiatomic NiTi alloy target, which exhibits an Ni-rich composition because the Ni sputtering yield is higher than that for Ti [33,34]. The content of all elements in the (TiVCr)N coatings remained at a constant value with various R_N. Coatings with an N content of about 50 at.% are regarded as saturated nitride coatings. The result is similar to the phenomena reported by Huang and Yeh [29]. Table 2 lists the variation of the deposition rate with R_N. The deposition rate increased slightly as R_N increased from 0% to 10%. This may be attributed to the incorporation of nitrogen or the formation of a loose structure, which is similar to the findings in several reported literature [35,36]. The deposition rate decreased from 12.38 to 5.60 nm/min

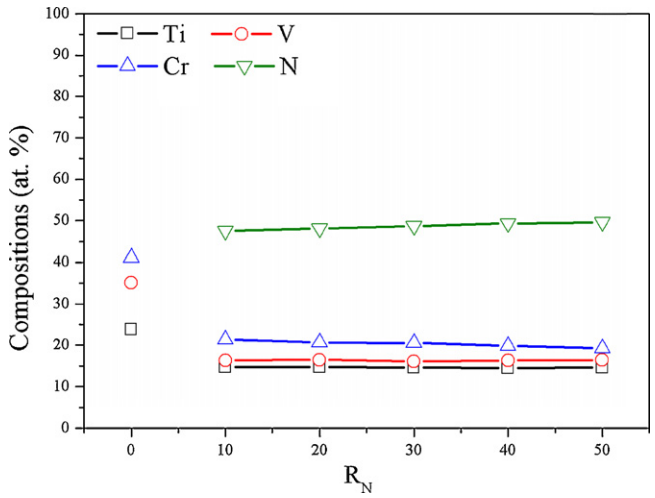

Fig. 1. EPMA element contents in (TiVCr)N coating deposited at various R_N.

Table 2
Relative intensities of diffraction peaks, average grain sizes and deposition rate of (TiVCr)N coatings.

R_N (%)	Relative intensity			Average grain size (nm)	Deposition rate (nm/min)
	(1 1 0)	(2 0 0)	(2 1 1)		
0	374.7	–	143.0	5.8	11.1
	(1 1 1)	(2 0 0)	(2 2 0)		
10	563.1	66.2	493.2	12.0	12.4
20	396.1	423.5	308.0	9.1	9.0
30	373.6	268.0	245.7	7.4	6.9
40	–	638.2	185.9	5.1	6.0
50	–	663.9	208.8	4.7	5.6

as the R_N increased from 10% to 50%. This phenomenon is a typical result of target poisoning. Moreover, the nitrogen ions are considered ineffective for sputtering compared with argon [37]. Therefore, the deposition rate decreased as R_N increased.

The XRD patterns of the (TiVCr)N coatings deposited at various R_N are shown in Fig. 2. The prominent peak from TiVCr alloy and nitride coatings could be indexed consistently based on the BCC and FCC [NaCl-type] phases, respectively. No traces of other phases were observed in the pattern. V and Cr are the BCC structures, whereas Ti is a BCC structure at 1150 K, which

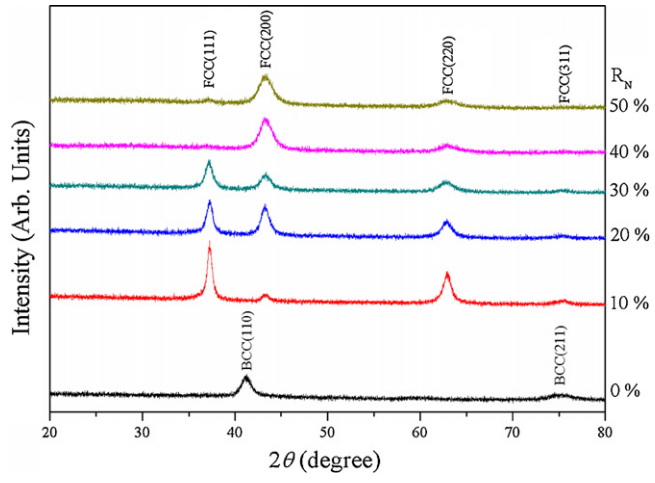

Fig. 2. X-ray diffraction pattern of the (TiVCr)N coatings deposited at various R_N.

Table 3
Interplanar spacing (d) and diffraction angle (2θ) of BCC (1 1 0) planes of individual elements and TiVCr alloy coatings as well as that of FCC (2 0 0) planes of individual nitrides and (TiVCr)N coatings deposited at R_N = 50%.

	Element			
	Ti	V	Cr	TiVCr
	Crystal structure			
	BCC	BCC	BCC	BCC
d (Å)	2.34	2.14	2.04	2.19
2θ (°)	38.48	42.17	44.39	41.22
	Nitride			
	TiN	VN	CrN	(TiVCr)N
	Crystal structure			
	FCC	FCC	FCC	FCC
d (Å)	2.12	2.07	2.07	2.09
2θ (°)	42.60	43.70	43.69	43.32

can be retained at room temperature by alloying with a small amount of elements, such as Nb or V [38]. Therefore, the mixed TiVCr alloy coatings tend to form a single BCC solid solution structure, as observed. The results found were similar to those by Tsai et al. and Cho et al. [31,39]. The (TiVCr)N coatings likely formed a single FCC solid solution structure because TiN, VN, and CrN were all FCC structures. The formation of the FCC solid solution is consistent with the phenomenon reported in other nitrides, such as Ti–Cr–N, Ti–Zr–N, Ti–Ta–N, Ti–V–N, Cr–V–N, and Zr–Y–N [14,15,17,40–42]. A single FCC structure has also been reported for the as-deposited multiprincipal element-nitrides, such as TiVCrZrY, AlCrTaTiZr, AlCrNbSiTiV, and TiAlCrNbY nitride coatings [27–30]. The angle of the (1 1 0) lattice plane for the TiVCr alloy coating or the (2 0 0) lattice planes for the (TiVCr)N coatings was close to the average value of mixed Ti, V, and Cr, or TiN, VN, and CrN, respectively, as listed in Table 3. This finding implies the formation of a solid solution from all constituted elements or nitrides.

In terms of crystallinity, strong (1 1 0) and weak (2 1 1) BCC peaks were initially observed for the metallic TiVCr alloy coatings deposited at R_N = 0%. This is explained by the fact that a (1 1 0) orientation is preferred for growth because a (1 1 0) lattice plane of a BCC phase has the lowest surface energy [43]. When R_N = 10%, the coatings showed a stronger (1 1 1) FCC orientation with relatively minor ones. However, when R_N = 20%, the (1 1 1) peak intensity decreased and the (2 0 0) peak intensity increased, implying a change in coating crystallography. Moreover, the (1 1 1) and (2 0 0) peak intensities decreased simultaneously at R_N = 30%. Note that grain size decreased as R_N increased to 30%. The coatings essentially had a complete (2 0 0) preferred orientation for R_N = 40% and R_N = 50%. The grain size further decreased with a considerable increase in R_N. The relative intensities of the diffraction peaks and average grain sizes of the (TiVCr)N coatings are listed in Table 2. Such pronounced change in the preferred orientation with an increase in R_N is explained by kinetics and thermodynamics. The preferred orientation is a consequence of the competition between neighboring grains. This competition leads to an evolutionary selection of the fastest-growing grains. Hence, the resulting preferred orientation corresponds to the orientation with the fastest growth rate in terms of geometry. In the case of the FCC [NaCl-type] structure, the (2 0 0) plane offers the lowest number of nearest neighbors to the incoming adatom and thus has the lowest growth rate in the viewpoint of kinetics. Conversely, (1 1 1) grains with the highest number of nearest interacting neighbors grow fastest. The (1 1 1) grains consequently expand slowly and overgrow all other grains. Associated with the shadowing effect-induced preferential depo-

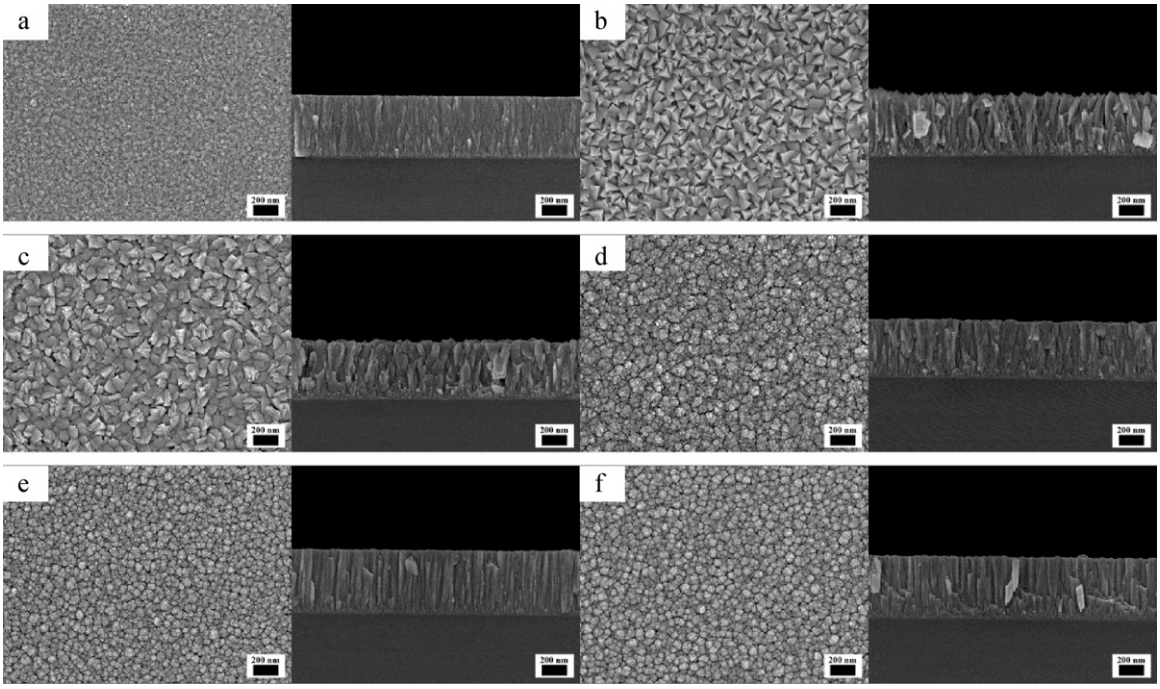

Fig. 3. Plan-view and cross-sectional SEM micrographs of the (TiVCr)N coatings deposited at various R_N: (a) 0, (b) 10, (c) 20, (d) 30, (e) 40, and (f) 50%.

sition, the difference is exacerbated. However, when sputtering at enough high R_N, the reactive gas acts as atomic N, which can originate from the N_2 dissociated in the gas phase or from N_2^+ ions accelerated toward the substrate that undergo collision-induced dissociation. In this situation, N spontaneously chemisorbs onto the nitride surface, subsequently forming a steady-state N coverage on the nitride surface itself. The plane with the lowest number of nearest neighbors changes from the (2 0 0) plane into the (1 1 1) plane, leading to a (2 0 0) preferred orientation growth [44–46]. The (2 0 0) plane has the lowest surface energy, as observed in the thermodynamic viewpoint [47]. Thus, the nitride coatings with high adatom mobility are expected to grow along the (2 0 0) orientation. The ion-to-atom ratio has a significant influence on adatom mobility during growth. Nitride growth under high ion-to-atom ratios gives more low-energy ion fluxes colliding with growing coating. Therefore, the (2 0 0) orientation prefers to grow at high R_N [48]. Moreover, an increase in R_N results in an increase in the proportion of energetic discharge species to deposited atoms at the growing coatings; this is mainly due to a decrease in the deposition rate [29]. When the energy flux is very high, even recrystallization or restructuring can occur. The whole coating then aims for its lowest surface energy. The combination of these effects results in a preferential growth of (2 0 0) grains, which is consistent with the results of this study.

Table 2 indicates that the average grain size of (TiVCr)N coatings decreases with increasing R_N. Interestingly, the relative intensities of diffraction peaks and average grain sizes of the TiVCr alloy coatings were less than those of the TiVCr nitride coatings deposited at R_N = 10%. For TiVCr alloy coatings, forming a highly crystallized solid solution structure is difficult due to the differences in the metallic elements in terms of atomic size and structure. In contrast, TiN, VN, and CrN have similar lattice constants and structures. The TiVCr nitride coatings deposited at R_N = 10% could therefore have higher crystallinity and larger grains than TiVCr alloy coatings. A similar investigation was reported in which the alloy coatings have an amorphous structure whereas the nitride coatings have an FCC crystal structure [28–30]. The coatings in this study were deposited at a substrate bias of −100 V. The energetic bombardments enhanced the mobility of lattice atoms in the deposited coatings, thereby improving film quality and increasing grain size. However, the excess energetic bombardments damaged the coatings during deposition and may have caused a self-resputtering effect [49,50]. As R_N increases, a greater proportion of energetic species to depositing atoms occurs in the growing coating. Therefore, the resputtering effect becomes relatively greater and consequently induces renucleation. As a result, the grain size continues to decrease with increasing R_N [51].

3.2. Microstructure development

Fig. 3 shows the plan-view and cross-sectional SEM micrographs of the (TiVCr)N coatings deposited at various R_N. All the (TiVCr)N coatings present uniform and homogenous structures. For the TiVCr alloy coatings, slightly faceted surface features and typical columnar structures were observed. The structure was quite compact and dense, which can be attributed to the application of substrate bias. A V-shaped columnar structure with a clearly faceted surface was obtained at R_N = 10%, which suggests the formation of a specific crystallography in these coatings. The grain size was then observed to have increased significantly. As R_N increased to 40% or 50%, the coatings exhibited a particular change in grain morphology, from strongly faceted pyramid-like grains to non-faceted spherical grains. This implies that recrystallization and restructuring took place at high R_N.

The plan-view and cross-sectional TEM micrographs with selected area diffraction (SAD) patterns of the (TiVCr)N coatings deposited at various R_N are shown in Fig. 4. All the coatings are uniform and there were no observable precipitations. A native amorphous SiO_2 layer was present at the interface between the Si wafer and the (TiVCr)N coatings. To reduce the surface energy, randomly oriented minute (TiVCr)N grains initially formed near the substrate surfaces and then tapered crystallites began to develop [52]. Similar to the aforementioned SEM observations, no visible void existed in the coating for TiVCr alloy coatings. A compact, dense columnar structure with indefinite boundaries was observed. The SAD patterns indicate the formation of a BCC crystal structure with a (1 1 0) preferred orientation. The coatings exhibited

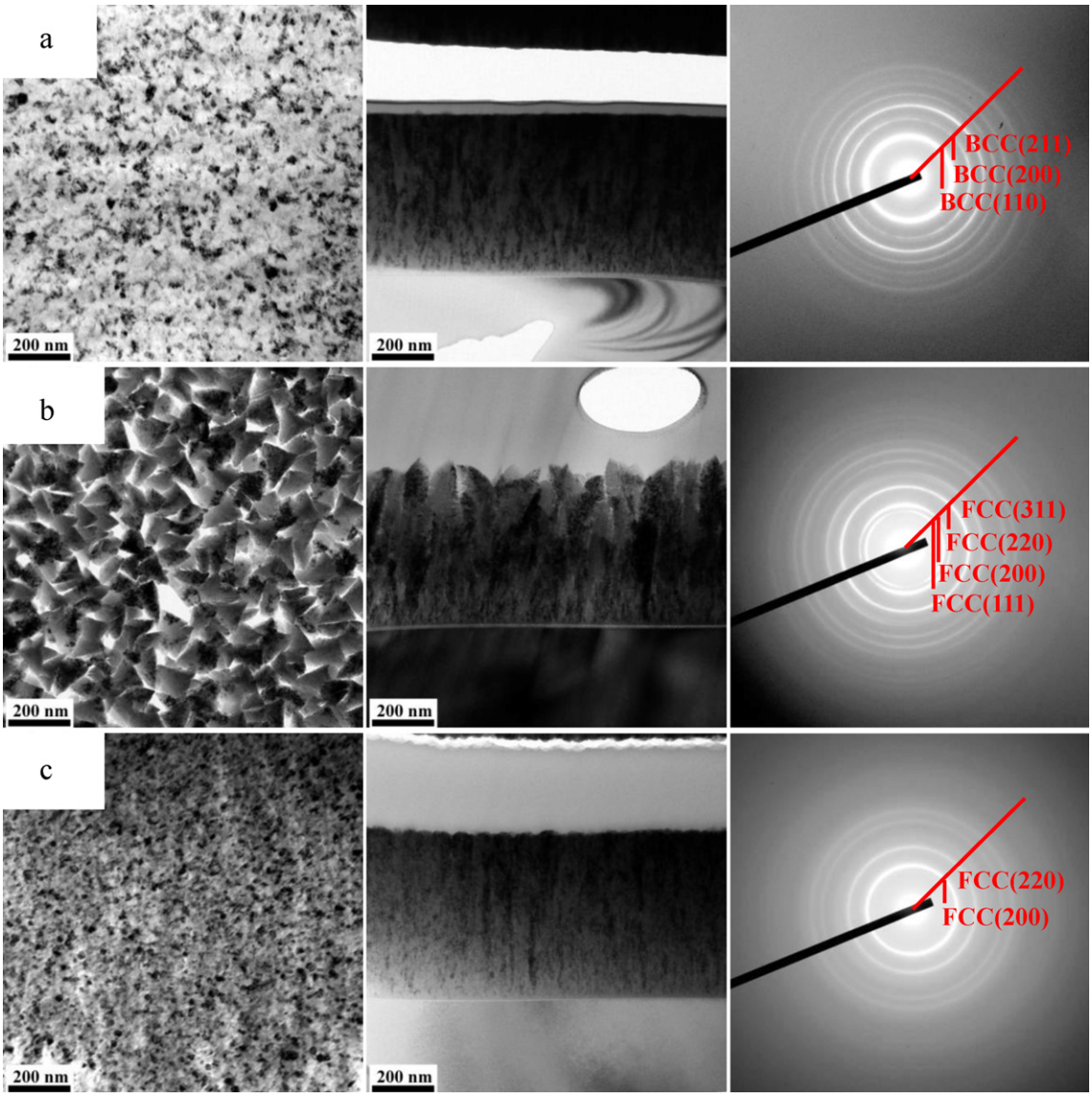

Fig. 4. Plan-view and cross-sectional TEM micrographs with SAD patterns of the (TiVCr)N coatings deposited at various R_N: (a) 0, (b) 10, and (c) 50%.

V-shaped columnar structures with faceted pyramid-like surfaces at R_N = 10%. A few micro and open voids were subsequently found in the coatings. As R_N continually increased to 40% or 50%, the V-shaped features and voids disappeared and the surface morphology transformed into a dome-like structure. In the SAD patterns of the TiVCr nitride coatings, diffraction rings corresponding to an FCC crystal structure were identified. However, for the coating deposited at R_N = 50%, a near complete (2 0 0) preferred orientation was observed. These results are consistent with the present XRD analysis.

The AFM images of the (TiVCr)N coatings deposited at various R_N are presented in Fig. 5. The surface roughness of the TiVCr alloy coating deposited at R_N = 0% was about 2.3 nm. At R_N = 10%, the surface roughness of the coatings increased to 14.9 nm due to the increasing size of the columnar structure. When R_N was further increased to 50%, densifications of the structure, as well as grain refinement occurred and the surface roughness decreased to 3.5 nm.

The microstructure of the sputtered coatings is influenced by many factors. In this study, the microstructure development can be represented as a function of R_N. The structure was likely dense and smooth for the TiVCr alloy coatings. The nitride formed at R_N = 10%, where a V-shaped columnar structure with a pyramid-like top surface and a much higher roughness of up to 14.85 nm were observed, implying the occurrence of an evolutionary overgrowth mechanism [53]. Due to the anisotropy of the growth rate on the crystallographic orientation, as previously mentioned, the fastest growing grains will overgrow all other grains. In other words, columns with the favored orientations will slowly emerge and kinetically overgrow the disadvantaged columns. The resulting coating will be characterized by V-shaped columns, all of which are faceted and have a preferred orientation, which correspond to the (1 1 1) orientation with fastest growth rate. In combination with the shadowing effect, the difference was exacerbated, resulting in high surface roughness and open column boundaries. When R_N was increased to 50%, the energy flux was so substantial that even recrystallization during grain growth occurred. Orientation selection was driven by lowering the surface energy of the whole coating as much as possible. As a result, the (2 0 0) grains consumed all other grains and straight, dome-like columns without any evolutionary V-shaped overgrowth formed the film [48]. However, the relatively larger resputtering effect increased the renucleation

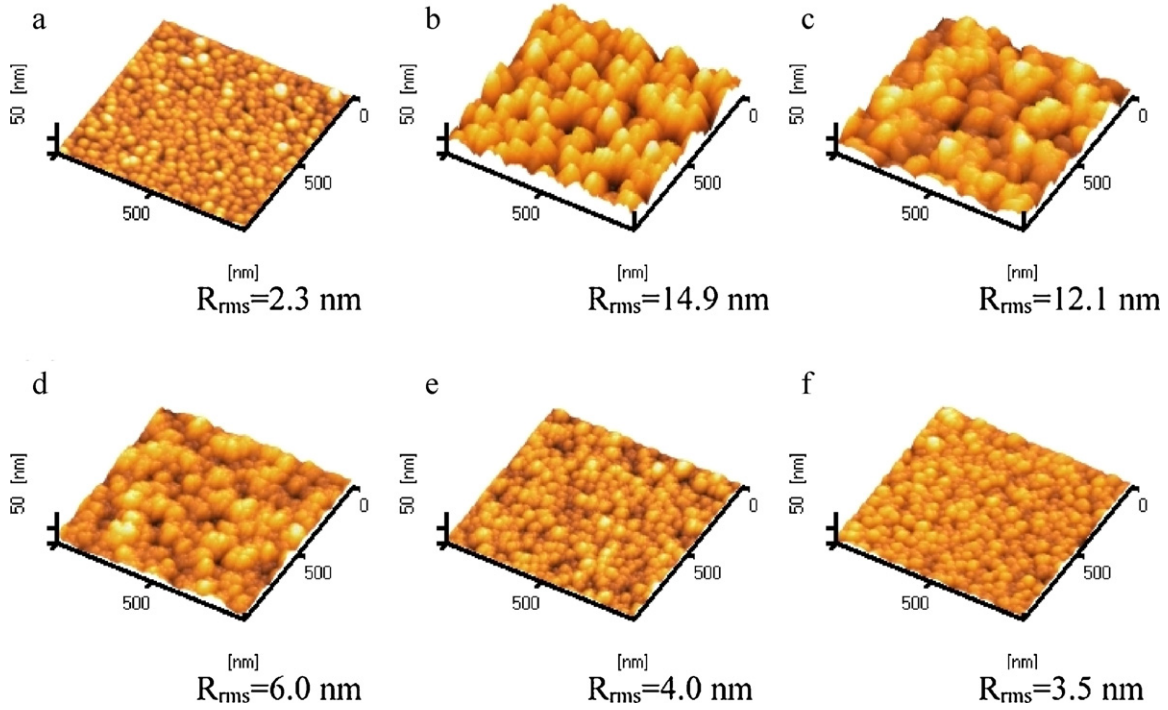

Fig. 5. AFM images of the (TiVCr)N coatings deposited at various R_N: (a) 0, (b) 10, (c) 20, (d) 30, (e) 40, and (f) 50%.

rate of the growing films, which in turn, inhibited grain growth [49–51].

3.3. Mechanical properties

The mechanical properties of the (TiVCr)N deposited at various R_N are plotted as shown in Fig. 6. The elastic modulus of the films basically followed the same trend as the hardness. The hardness of the TiVCr alloy coatings reached 12.60 GPa, higher than that of typical pure metal and alloy coatings (i.e., Ti, ~4.5 GPa; V, ~2.6 GPa; Cr, ~4.7 GPa; Zr–Cu, ~4.0 GPa; Zr–Cu–Ti, ~6.6 GPa; Ni–Ti, ~8.0 GPa; Al–Ti, ~9.0 GPa; and Zr–Y, ~6.0 GPa) due to the solid solution strengthening effect provided by the incorporation of atoms having different sizes [3,42,54–56]. However, the hardness decreased by 8.54 GPa when R_N increased from 0% to 10%. This can be attributed mainly to the high density of the voids between the columns due to the evolutionary overgrowth mechanism. As

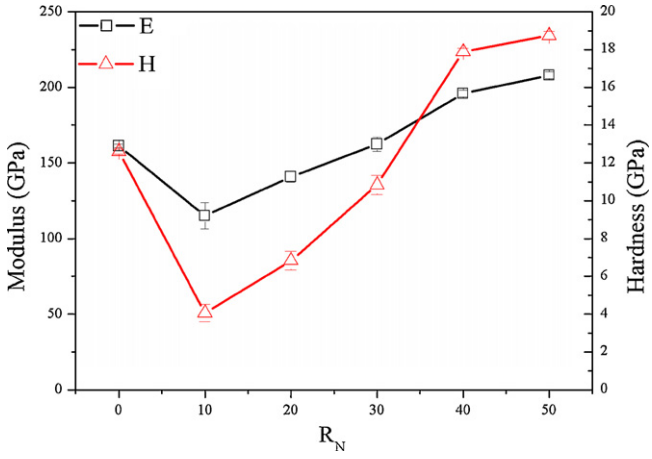

Fig. 6. Hardness and elastic modulus of the (TiVCr)N coatings deposited at various R_N.

R_N increased from 10% to 50%, the hardness increased from 4.06 to 18.74 GPa. The mechanical properties of the films were enhanced because the strong bombardment of the growing films at high R_N markedly reduced the density of the voids existing between the column structures [27,57]. Grain refinement also has an effect when the mechanical properties were increased. These impede atomic migration and hamper boundary sliding during plastic deformation. The densification of the structure and the grain refinement were then considered as the main contributors to the increased hardness.

4. Conclusions

In this study, (TiVCr)N coatings were prepared by reactive magnetron sputtering of a pure equimolar TiVCr target on Si (1 0 0) wafers at R_N ranging from 0% to 50%. Our results indicate that the elemental sputtering yield in the TiVCr alloy, which was not reported in the literature, followed the sequence Cr > V > Ti. The deposition rate gradually decreased with increasing R_N. The deposited TiVCr alloy and nitride coatings possessed BCC and FCC solid solution structures, respectively, rather than multiphase complex structures. The TiVCr alloy coating deposited at R_N = 0% exhibited a very dense and smooth columnar structure with a (1 1 0) preferred orientation, whereas the (TiVCr)N coating deposited at R_N = 10% had a V-shape columnar structure with open void boundaries. Highly faceted features were observed on the surface, especially for the coatings with strong (1 1 1) preferred orientations. The microstructure of the (TiVCr)N coatings is evolved through the competitive growth between adjacent (1 1 1)- and (2 0 0)-oriented grains, which is typical of an evolutionary overgrowth mechanism. As the R_N was increased from 10% to 50%, the microstructure of the coatings visibly changed to denser and smaller columns with domed surfaces. The change in the preferred orientation from (1 1 1) to (2 0 0) was also observed. As indicated by TEM cross-sections, no evolutionary overgrowth that corresponds to recrystallization and restructuring occurred. The hardness and elastic modulus of the nitride coatings deposited at R_N = 50% were

enhanced to 18.74 and 208.06 GPa, respectively. This is attributed to the densification of the structure and the grain refinement.

Acknowledgement

The authors gratefully acknowledge the financial support for this research by the National Science Council of Taiwan under grant no. NSC99-2221-E-005-025-MY3.

References

[1] H.O. Pierson, Handbook of Refractory Carbides and Nitrides, Noyes, New Jersey, 1996.
[2] Y. Xi, H. Fan, W. Liu, J. Alloys Compd. 496 (2010) 695–698.
[3] A. Kumar, D. Singh, R. Kumar, D. Kaur, J. Alloys Compd. 479 (2009) 166–172.
[4] J.L. Ruan, D.F. Lii, H.H. Lu, J.S. Chen, J.L. Huang, J. Alloys Compd. 478 (2009) 671–675.
[5] L. Chen, Y. Du, S.Q. Wang, A.J. Wang, H.H. Xu, Mater. Sci. Eng. A 502 (2009) 139–143.
[6] Y.C. Chim, X.Z. Ding, X.T. Zeng, S. Zhang, Thin Solid Films 517 (2009) 4845–4849.
[7] M. Keunecke, C. Stein, K. Bewilogua, W. Koelker, D. Kassel, H. van den Berg, Surf. Coat. Technol. 205 (2010) 1273–1278.
[8] X.Z. Ding, X.T. Zeng, Y.C. Liu, F.Z. Fang, G.C. Lim, Thin Solid Films 516 (2008) 1710–1715.
[9] J.T. Chen, J. Wang, F. Zhang, G.A. Zhang, X.Y. Fan, Z.G. Wu, P.X. Yan, J. Alloys Compd. 472 (2009) 91–96.
[10] Y. Chunyan, T. Linhai, W. Yinghui, W. Shebin, L. Tianbao, X. Bingshe, Appl. Surf. Sci. 255 (2009) 4033–4038.
[11] X. Wang, L.S. Wang, Z.B. Qi, G.H. Yue, Y.Z. Chen, Z.C. Wang, D.L. Peng, J. Alloys Compd. 502 (2010) 243–249.
[12] P. Budzynski, J. Sielanko, Z. Surowiec, P. Tarkowski, Vacuum 83 (2009) S186–S189.
[13] D.B. Lee, M.H. Kim, Y.C. Lee, S.C. Kwon, Surf. Coat. Technol. 141 (2001) 232–239.
[14] V.M. Vishnyakov, V.I. Bachurin, K.F. Minnebaev, R. Valizadeh, D.G. Teer, J.S. Colligon, V.V. Vishnyakov, V.E. Yurasova, Thin Solid Films 497 (2006) 189–195.
[15] Y.W. Lin, J.H. Huang, G.P. Yu, Thin Solid Films 518 (2010) 7308–7311.
[16] K.P. Purushotham, L.P. Ward, N. Brack, P.J. Pigram, P. Evans, H. Noorman, R.R. Manory, Wear 254 (2003) 589–596.
[17] G. Abadias, L.E. Koutsokeras, S.N. Dub, G.N. Tolmachova, A. Debelle, T. Sauvage, J. Vac. Sci. Technol. A 28 (2010) 541–551.
[18] S.M. Kim, B.S. Kim, G.S. Kim, S.Y. Lee, B.Y. Lee, Surf. Coat. Technol. 202 (2008) 5521–5525.
[19] J.W. Yeh, S.K. Chen, S.J. Lin, J.Y. Gan, T.S. Chin, T.T. Shun, C.H. Tsau, S.Y. Chang, Adv. Eng. Mater. 6 (2004) 299–303.
[20] P.K. Huang, J.W. Yeh, T.T. Shun, S.K. Chen, Adv. Eng. Mater. 6 (2004) 74–78.
[21] C.J. Tong, M.R. Chen, S.K. Chen, J.W. Yeh, T.T. Shun, S.J. Lin, S.Y. Chang, Metall. Mater. Trans. A 36A (2005) 1263–1271.
[22] C.J. Tong, Y.L. Chen, S.K. Chen, J.W. Yeh, T.T. Shun, C.H. Tsau, S.J. Lin, S.Y. Chang, Metall. Mater. Trans. A 36A (2005) 881–893.
[23] C. Li, J.C. Li, M. Zhao, Q. Jiang, J. Alloys Compd. 504S (2010) S515–S518.
[24] B.S. Li, Y.P. Wang, M.X. Ren, C. Yang, H.Z. Fu, Mater. Sci. Eng. A 498 (2008) 482–486.
[25] F.J. Wang, Y. Zhang, G.L. Chen, J. Alloys Compd. 478 (2009) 321–324.
[26] T.T. Shun, C.H. Hung, C.F. Lee, J. Alloys Compd. 493 (2010) 105–109.
[27] D.C. Tsai, Y.L. Huang, S.R. Lin, S.C. Liang, F.S. Shieu, Appl. Surf. Sci. 257 (2010) 1361–1367.
[28] S.Y. Chang, S.Y. Lin, Y.C. Huang, C.L. Wu, Surf. Coat. Technol. 204 (2010) 3307–3314.
[29] P.K. Huang, J.W. Yeh, Surf. Coat. Technol. 203 (2009) 1891–1896.
[30] M. Braic, V. Braic, M. Balaceanu, C.N. Zoita, A. Vladescu, E. Grigore, Surf. Coat. Technol. 204 (2010) 2010–2014.
[31] D.C. Tsai, F.S. Shieu, S.Y. Chang, H.C. Yao, M.J. Deng, J. Electrochem. Soc. 157 (2010) K52–K58.
[32] H.P. Klug, L.E. Alexander, X-ray Diffraction Procedures for Polycrystalline and Amorphous Materials, Wiley & Sons, New York, 1974.
[33] N. Laegreid, G.K. Wehner, J. Appl. Phys. 32 (1961) 365–369.
[34] K.N. Melton, Engineering Aspects of Shape Memory Alloys, Butterworth-Heinemann, London, 1990.
[35] L.F. Donaghey, L.G. Geraghty, Thin Solid Films 38 (1976) 271–280.
[36] M. Yoshitake, K. Takiguchi, Y. Suzuki, S. Ogawa, J. Vac. Sci. Technol. A 6 (1988) 2326–2332.
[37] R.M. Mason, M. Pichiling, J. Phys. D: Appl. Phys. 27 (1994) 2363–2371.
[38] A.J. Maeland, G.G. Libowitz, J.F. Lynch, J. Less Common Met. 104 (1984) 361–364.
[39] S.W. Cho, C.N. Park, J.H. Yoo, J. Choi, J.S. Park, C.Y. Suh, G. Shim, J. Alloys Compd. 403 (2005) 262–266.
[40] M. Uchida, N. Nihira, A. Mitsuo, K. Toyoda, K. Kubota, T. Aizawa, Surf. Coat. Technol. 177–178 (2004) 627–630.
[41] H. Hasegawa, A. Kimura, T. Suzuki, J. Vac. Sci. Technol. A 18 (2000) 1038–1040.
[42] J. Musil, H. Polàkovà, Surf. Coat. Technol. 127 (2000) 99–106.
[43] M. Lu, J.H. Judy, J.M. Sivertsen, IEEE Trans. Magn. 26 (1990) 1581–1583.
[44] J.E. Greene, J.-E. Sundgren, L. Hultman, I. Petrov, D.B. Bergstrom, Appl. Phys. Lett. 67 (1995) 2928–2930.
[45] L. Hultman, J.-E. Sundgren, J.E. Greene, D.B. Bergstrom, I. Petrov, J. Appl. Phys. 78 (1995) 5395–5403.
[46] D. Gall, S. Kodambaka, M.A. Wall, I. Petrov, J.E. Greene, J. Appl. Phys. 93 (2003) 9086–9094.
[47] J. Pelleg, L.Z. Zevin, S. Lungo, N. Croitoru, Thin Solid Films 197 (1991) 117–128.
[48] S. Mahieu, P. Ghekiere, G.D. Winter, R.D. Gryse, D. Depla, G.V. Tendeloo, O.I. Lebedev, Surf. Coat. Technol. 200 (2006) 2764–2768.
[49] H.C. Yao, M.C. Chiu, W.T. Wu, F.S. Shieu, J. Electrochem. Soc. 153 (2006) F237–F243.
[50] K.J. Martin, A. Madan, D. Hoffman, J. Ji, S.A. Barnett, J. Vac. Sci. Technol. A 23 (2005) 90–98.
[51] J.C. Lin, G. Chen, C. Lee, J. Electrochem. Soc. 146 (1999) 1835–1839.
[52] S.H. Kim, Y.L. Choi, Y.S. Song, D.Y. Lee, S.J. Lee, Mater. Lett. 57 (2002) 343–348.
[53] A. van der Drift, Philips Res. Rep. 22 (1967) 267–288.
[54] E. Blando, R. Hubler, Surf. Coat. Technol. 158–159 (2002) 685–689.
[55] H.S. Chou, J.C. Huang, L.W. Chang, T.G. Nieh, Appl. Phys. Lett. 93 (2008), 191901-1-1191901.
[56] J. Hampshire, P.J. Kelly, D.G. Teer, Thin Solid Films 447–448 (2004) 392–398.
[57] C.K. Chung, T.S. Chen, J. Mater. Res. 23 (2008) 494–499.